UNIVERSITY OF LEEDS

This is a repository copy of *Design of a steady-state in situ test to determine the air permeability coefficient of covercrete*.

White Rose Research Online URL for this paper:
http://eprints.whiterose.ac.uk/137958/

Version: Accepted Version

Article:
Yang, K orcid.org/0000-0002-4223-2710, Wang, Y, Long, A et al. (3 more authors) (2019) Design of a steady-state in situ test to determine the air permeability coefficient of covercrete. Construction and Building Materials, 195. pp. 671-681. ISSN 0950-0618

https://doi.org/10.1016/j.conbuildmat.2018.10.200

(c) 2018, Elsevier Ltd. This manuscript version is made available under the CC BY-NC-ND 4.0 license https://creativecommons.org/licenses/by-nc-nd/4.0/

Reuse
This article is distributed under the terms of the Creative Commons Attribution-NonCommercial-NoDerivs (CC BY-NC-ND) licence. This licence only allows you to download this work and share it with others as long as you credit the authors, but you can't change the article in any way or use it commercially. More information and the full terms of the licence here: https://creativecommons.org/licenses/

Takedown
If you consider content in White Rose Research Online to be in breach of UK law, please notify us by emailing eprints@whiterose.ac.uk including the URL of the record and the reason for the withdrawal request.

White Rose university consortium
Universities of Leeds, Sheffield & York

eprints@whiterose.ac.uk
https://eprints.whiterose.ac.uk/

Design of a steady-state in situ test to determine the air permeability coefficient of covercrete

Kai Yang[a,b], Yaocheng Wang[c*], Adrian Long[c], Changhui Yang[a], Song Mu[e] and Muhammed Basheer[b]

a: College of Materials Science and Engineering, Chongqing University, Chongqing, China

b: School of Civil Engineering, University of Leeds, Leeds, UK

c: School of Civil Engineering, Shenzhen University, China

d: School of Natural and Built Environment, Queen's University Belfast, UK

e: State Key Laboratory of High Performance Civil Engineering Materials, Nanjing, China

Abstract

An in situ air permeability test method that does not require assumptions for the often-difficult unidirectional flow has been developed to calculate the air permeability coefficient of the near surface concrete. The proposed method involves applying a constant pressure head to a surface mounted ring and measuring the steady state air flow rates. The analysis is based on modification of the flownet theory, which needs a calibration factor accounting for the influence of specimen and ring geometries. Effects of test area, width of seal, depth and width of test specimen were investigated using numerical simulation of the air flow. The repeatability of the proposed test method was assessed by the signal noise ratio (SNR) and discrimination ratio (DR). A new formula is offered and it only requires the steady state air flow rate to calculate the coefficient of air permeability, thus assisting engineers and researchers to quickly determine this property of structural concretes.

Key words: flownet, steady-state state, in situ air permeability test, covercrete, repeatablity, reliability

1. Introduction

The assessment of permeability is of great importance for many scientific and practical problems associated with the use of concrete in many projects, e.g. concrete property optimisation, structural quality control, and service life prediction [1-3]. In situ air permeability test methods offer considerable advantages in terms of many criteria deemed to be important for field assessment of permeability and are rapidly becoming a commonly accepted method for determining permeation properties of structural concrete. In this respect, they have proven to be useful for characterising site quality and potential durability of concrete in structure [4-6].

Following the early work of Glanville in 1930s [7] and Figg in 1970s [8], other researchers introduced numerous methods for assessing the permeability of structural concrete [5, 6, 9-12], which can be grouped under surface mounted tests and drill-hole tests. In spite of remarkable variations of these methods, such as testing procedures, capabilities, and complexity, the fundamental principle of most methods is the same, which is based on non-steady state flow analysis for reasons of simplicity. Semi-empirical calculations based on measurements carried out allow the determination of the air permeability in a fairly consistent quantitative way. However, in most cases, it is only possible to obtain a permeability index [7-15], and the coefficients of air permeability cannot be estimated due to inherent limitations. That is, the results from these tests cannot be directly used in service life prediction models and a comparison of air permeability from different test methods is not easy. These limitations significantly limit the extent of their application.

The empirical theories used in some of these test methods assume that a uni-directional flow is reached and the accessible porosity used in the governing equation is regarded as a constant or embedded into the permeability index obtained from the tests [12, 16]. Clearly, these hypothesises are not true for field measurements and hence, no in situ method is currently available for determining the steady state air permeability coefficient. Although a guard-ring is sometimes used to achieve the uni-directional flow in the test region and to increase the effective test region [9, 17, 18], it is still debatable whether its benefits over other test arrangements justify the higher complexity associated with the test set up using guard rings. Yang et al. [19] have shown that the flow features are significantly affected by

various factors including configurations of the test setup and test locations. Even under the best circumstances, only the central portion of the guard ring approximates a true one-dimensional flow.

The steady-state analysis, normally not taken into consideration in field test techniques, has many scientific and technological advantages. It minimises the effect of both multi-directional flow and variations in porosity with depth, both of which avoid two unreliable assumptions highlighted previously [19-22]. Whiting and Cady [23] developed a field test to measure the steady-state air flow rate under vacuum, but no analytical solution to obtain an air permeability coefficient was given. Against these backgrounds, it has been established that the development of a rapid, non-destructive, in situ air permeability test is highly appropriate.

Therefore, the objective of this study was to develop a steady-state air permeability test, by putting emphasis on determining the steady state air permeability coefficient, which incorporates the advantages of current field test methods whilst addressing their limitations. To achieve this, the flownet theory was used to analyse simulated flow patterns and estimate the calibration factor to be used in the calculation of the steady state air permeability coefficient. A test instrument for measuring the air flow rate was designed and the influence of the applied pressure on the duration to reach the steady state was investigated. These data were used to clarify the effects of key parameters on the proposed test method. Finally, the reliability of the proposed method was examined by the discrimination ratio (DR) and the signal-noise ratio (SNR) recommended by ISO [24] and Automotive Industry Action Group (AIAG) [25, 26].

2. Governing equation to determine the steady state air permeability coefficient

The flownet theory, which was used to determine the coefficient of water permeability of concrete in the CLAM water permeability test [21], is sufficiently versatile to be applied to the steady-state air permeability test. The method involves the establishment of a flownet that consists of equipotential lines and flow lines, as indicated in **Figure 1**. An equipotential line is one for which all points have the same value of potential; on a flow line, all points have the same value of flow. The air flow through concrete is described by the flownet and the geometry patterns are used to obtain the analytical solution

for determining the steady state air permeability coefficient. The relationship between the permeability coefficient and the steady state flow rate can be expressed by:

$$K_{air} = q \times \frac{1}{2\pi h_t} \times \frac{n_d}{n_f} \times \frac{l}{rb} = q \times C \quad (1)$$

where K_{air} is the air permeability coefficient (m/s); q is the steady-state air flow (m^3/s); h_t is the head applied (m); n_f is the number of paths (flow channels); n_d is the number of equipotential drops; r is the distance normal to symmetry axis (m); b is the width of flow path (m); l is the distance between equipotential lines (m); $\frac{1}{2\pi h_t} \times \frac{n_d}{n_f} \times \frac{l}{rb}$ is considered as the calibration factor (C), which is a function of only the flow geometry.

Verification of the flownet theory has been previously reported by several researchers [19, 21, 22]. Note that the earlier studies dealt only with water flow simulation through the surface mounted test [19, 27], whilst the present work concerns air flow. Therefore, the flow rate measured under different test pressures have to be converted into the flow rate at the ambient test condition, because the volume flow rate depends on the test pressure due to air compressibility.

3. Flow simulation to evaluate the value of calibration factor (C)

The flow simulation is not only helpful to optimise the design of the instrument, but also useful to establish approaches to interpret test results. The finite element analysis (FEA) provides a valuable means to achieve this [19]. Our previous research [21, 27] has shown that the steady state flow pattern is a function of the material characteristics and when the permeability of the near-surface concrete (the top layer of concrete from the surface to 5mm depth) is 3 times higher than the inner concrete, the steady state flow path is not sensitive to the permeability gradient. Against this background, the concrete was considered as a homogenous porous material with uniform permeability in the simulation and the air flow simulation was carried out to clarify the influence of geometric configurations of the specimen and the instrument on the flownet.

Figure 2 illustrates the input boundary conditions and the output of the simulation. **Figure 2-a** shows the x and y-axes imposed to define a specimen and the plate that represents the cross section of the specimen. **Figure 2-b** plots the air flow patterns, described by equi-potentials and air flow lines. More specifically, the following four factors are taken into account:

1) depth of the specimen (d_{sp})
2) width of the specimen (w_{sp})
3) radius of the testing area (r_{ta})
4) width of the seal around the central test region (s_w)

A factorial experiment design was carried out to investigate the effect of the above four factors, details of which are summarised in **Table 1**, and air flow models were built. In developing the flownet for a given condition, the orthogonality condition must be satisfied and producing an acceptable solution is largely a matter of trail and error, which, in turn, is a function of the experience and patience [21, 22, 27]. On the basis of the flownets, the calibration factor (C) was evaluated. The procedure used closely followed the programs previously developed [19, 27] and the results of the calibration factor were interpreted through factorial experiment analysis [25, 26].

Table 2 summarises results of the factorial analysis and **Figure 3** plots the main effects of four factors. The statistical analysis reveals that the effect of the radius has a significant influence on the calibration factor; the greater the radius, the lower the calibration factor (**Figure 3-a**). As indicated in **Figure 1**, an increase in the radius of the test area would increase the distance normal to the axis of symmetry (r) and the width of the flow path (b), which naturally lead to an overall decrease of l/rb. The results also indicate that values of the calibration factor are not strongly affected by changes of other factors, suggesting that a relatively consistent flownet can be achieved for all other combinations. It needs to be highlighted that only two levels of the factors were investigated and the conclusions were valid within the boundaries specified in **Table 1**. **Table 2** gives details of the two-way interactions between the four factors investigated; as can be seen there existed no strong interactions [28]. On the basis of the results obtained in this study and the previous research [5, 19], it was decided to design the instrument with 25 mm test area radius. This can be justified with the following three reasons: firstly,

when the test area was large (using the 37.5mm radius test head), the test results indicated a low reliability and high variability; secondly, the maximum size of coarse aggregate is around 20mm in most cases and the diameter of test area should be 2.5 times this to eliminate the heterogeneous nature of concrete [12, 17]; and thirdly, the holding force required to seal the test head on the concrete surface for site applications needs to be as low as possible. In addition, to avoid the influence of a high permeable top layer on air flow measurements, the width of the seal around the central test region was specified as 30 mm thereby forcing air to pass through deeper part of the cover zone [6, 9, 23, 29].

Once the geometric parameters of the test instrument were determined, further investigations were carried out to refine the influence of boundary conditions of the specimen on measured air flow rate. It was intended to estimate potential correction factors under certain practical conditions, e.g. assessment of the permeability of either thin concrete elements or closer to their edge. Therefore, another 11 numerical models were built to examine the influence of specimen thickness and distance between the edge of the test head and the edge of the specimen. The flow simulation results are displayed in **Figure 4**.

As shown in **Figure 4-a** to **f**, the specimen depth has a significant influence on the flow pattern, especially for depths less than 50 mm (**Figure 4-a1** and **b1**), as confirmed previously for the steady state water permeability test by Adams and Arbaoui [21, 28]. The equi-potential lines locate right below the testing area for a thinner specimen, indicating that most air transports perpendicular to the test surface. This is because air tends to flow through the shortest paths and the direction perpendicular to the surface of the thin specimen matches this requirement. As the depth of the specimen increases, the air flow perpendicular to the test surface reduces. Furthermore, no significant difference in flow patterns can be found as the depth is beyond 50 mm. **Figure 5-a** gives the relationship between the calibration factor and the depth of the specimen. Obviously, an increase in specimen depth caused an increase in calibration factor, but reached a relatively constant value (0.051 mm^{-1}) beyond 50 mm. This is mainly due to rapid changes in the relative proportion of the flow parallel to the test surface and the growth of the l component (as shown in **Figure 1**), both yielding a higher calibration factor. Interpretation of the flownets in **Figure 4-a** to **f** also reveals that equi-potential lines locate closely

around the edge of the test area. This means a higher pressure gradient and hence a higher proportion of flow lines parallel to the test surface in these cases. The above result agrees well with the previous findings by Bamforth [21] and Arbaoui [26]. With reference to **Figures 3** and **4**, the correction of calibration factor should be only made if the depth of the testing member is less than 50 mm.

Figure 4-g to **k** along with **d** give the results of air flow simulation with different distances to the out ring and **Figure 5-b** plots the calibration factor against the distance between the test area and the outer edge of the test specimen. Note that in these figures, the depth was kept at a constant value (100 mm) to avoid additional variations in the calibration factor. It was found that the distance to the outer side of the test specimen did not have a noticeable effect on the flownet in comparison to the effect of the specimen depth. This trend is also clearly reflected in low variations in the calibration factors, as indicated in **Figure 5-b**. Parrott and Hong [6] investigated the effective testing volume of concrete and the air permeated area. Their investigation also highlighted that the region influencing the air permeability test is mainly about 20 mm around the testing area, which is similar to the results here. For this reason, it was concluded that there is no need to correct the calibration factor for the distance from the test region to the outer edge of the specimen, provided there is at least 20mm between the test head and the outer edge of the test specimen.

4. Design of the in situ air permeability test instrument

The air permeability is calculated according to the flownet theory, which requires the value of the steady-state air flow rate (given in **Eq 1**). To verify this concept, it was necessary to manufacture a test prototype to obtain the value of the steady state flow rate. **Figure 6** shows the air permeability test setup and it contains three main parts: a test head, a measuring body and a priming system, which is similar to the high-pressure water permeability test reported previously [16, 19, 30]. The test head is shown in **Figure 6-a** with one bleed valve located at the centre of the head. **Figure 6-b** shows the measuring unit, which consists of three parts: a power supply, a display box and a testing unit. The testing unit is connected to the test head and the control box. The display box has a digital panel that shows the volume of air flowing into the concrete through the test area and the pressure levels at the test area. The air pressure is increased using the priming system, shown in **Figure 6-c**. It comprises an

air compressor, an air reservoir with a pressure gauge and a pressure regulator. In order to maintain the constant testing pressure, a high precision pressure regulator was used, which was set to the desired pressure level prior to measurements.

As inferred from the results of the air flow simulation, the circular testing area with a radius of 25 mm was chosen, offering a representative testing area for most structural concrete [9, 20, 31, 32]. This was achieved by using a 110 mm diameter aluminium plate fitted with a 5 mm thick natural rubber ring isolating a circular flow area. In this study, it was decided to force air to flow through concrete under an applied pressure above atmospheric using an air compressor. This is mainly because the previous studies [11, 33] have indicated that the rate of air flow under vacuum is generally lower than that under an over-pressure and hence the air permeability test under vacuum might decrease the sensitivity of the test method. Furthermore, previous results [34] have shown that when a high vacuum (240mm Hg) is applied, moisture from the inner section of concrete moves to the surface which can affect the results. Therefore, in this research, the steady state air permeability test was developed by applying an over-pressure instead of vacuum.

5. Experimental programme

The experimental work was intended to verify the proposed theory under different testing conditions and assess the performance of the constant head (air pressure) air permeability test instrument. To achieve this objective, the influence of test pressure on duration to reach a steady state flow rate was investigated first, followed by establishing the relationship between the test pressure and the steady-state flow rate. The third part was to justify whether or not the repeatability of the proposed test method is acceptable according to the discrimination ratio (DR) and the signal-noise ratio (SNR).

5.1 Preparation of the test specimens

The concrete investigated was manufactured with a water-cement ratio of 0.35 and a mix proportion of 1:1.44:2.56 between cement, sand and coarse aggregate. The concrete was manufactured with CEM-I 42.5N Portland cement, medium natural sand (fineness modulus: 2.60, specific gravity: 2.52), 10 mm and 20 mm size basalt coarse aggregate (specific gravity: 2.65) in a 1:1 proportion by weight. Dried

aggregates were used and a predetermined allowance for their water absorption was made to the total water used in the mix. A polycarboxylic acid based superplasticiser was used to achieve the target workability. The mixing was carried out according to BS-1881: part 125 [35]. After mixing, the slump was and air content were determined according to GB-50082 [36], which were 210 mm and 1.6% respectively.

The test specimens were blocks of size 300×250×150 mm and the proposed air permeability tests were carried out on the 300×250 mm mould finished surface. After compaction, the specimens were immediately covered with plastic sheets to prevent the evaporation of water from the freshly placed concrete. The blocks were removed from their mould after 1 day and were cured until the age of 90 days by following the two procedures below:

1) Air cured (AC): air-stored in a controlled environment (20 ± 2 ^{o}C, 50 ± 10% RH) after demoulding.
2) Moisture cured (MC): transferred into a fog room (20 ± 2 ^{o}C) after demoulding until test.

Two curing regimes were designed to offer different permeability properties, especially for the near surface region. Note that prior to carrying out air permeability measurements, the slabs were dried in an oven at 40 ^{o}C for 28 days after curing. This drying regime was selected based on results of previous studies in order to remove the influence of moisture on the results [37, 38], in which it was established that most of the free moisture is removed after 3-weeks of drying and no signficant influence of moisture gradient on air permeability test is found.

5.2 BS-EN water penetration test

Water penetration test, according to BS-EN: 12390-8 [39] was carried out on 100mm diameter cores cut from the test blocks after carrying out the air permeability measurements. Water was admitted at a constant test pressure of 7.0 bar for 3 days at one end of the test specimen. At the end of the test, specimens were split open and the depth of water penetration was measured. The average value of three replicates is reported. The values thus obtained were then compared with the effects identified using the proposed air permeability test so that the reliability of the latter could be established.

5.3 Steady state air permeability test

The test set up shown in **Figure 6** was used to carry out the in situ surface mounted air permeability test. Before clamping the test head on the specimen to be tested, the air tightness of the test head was checked by mounting it on a plane metal plate and applying air under pressure through the priming system. If there was no pressure drop, this indicated that the test head did not have any leak. Then, the test head was mounted on the concrete surface and connected to both the measuring unit and the priming system. The valves of the priming system (**Figure 6-c**) were kept opened and the air compressor was switched on to apply pressure in the air reservoir. The pump was turned off when the pressure gauge reading was slightly above the specified pressure. The initial volume reading was recorded (t=0 min). At this test pressure air penetrated into the concrete, which resulted in a decrease of the pressure inside the chamber. The pressure was maintained at the specified pressure by advancing the piston, which allowed the volume of air entering in to the concrete to be recorded at every minute. The air flow rates were computed from the movement of the piston and the diameter of the cylinder. A test duration of 60 mins was selected, during which the air flow rate was considered to have reached a steady state of flow. The instrument has two distinctive features, viz. maintaining a constant testing pressure and measuring the flow rate accurately.

6. Results and Discussion

6.1 The effect of test pressure and curing regime on air flow response

To identify the influence of test pressure on the air flow, the flow rates were monitored continuously, which were used to identify the duration at which the steady state was achieved. **Figure 7** shows the plot of the recorded air flow rates under different pressure levels, with each data point representing the average value of 3 replicates at different locations. As shown in **Figure 7**, strong fluctuations of air flow are observed at the beginning which is generally considered as the non-steady state. Another feature is that the length of the non-steady state stage mainly depended on the test pressure applied and the type of concrete tested. More specifically, it took 30 minutes to achieve the steady state when the testing pressure was 0.5 bar for the two concretes, whereas at 1.2 bar the air flow rates became constant within 20 minutes. This means that the increase of test pressure from 0.5 bar to 1.2 bar can significantly

shorten the duration (from 30 minutes to 20 minutes) to get the steady state rate of flow. This trend, however, was less pronounced, when test pressure was further increased to 2 bar, as the time needed to achieve a steady-state did not show a significant reduction. The steady state flow is attained when the flownet is established within the test region and it is common that a high pressure can accelerate the process of establishing the flow patterns [22, 23, 40]. As a result, increasing the testing pressure led to the reduction of time needed for a steady state. However, a further decrease was not observed when the pressure was increased from 1.2 bar to 2 bar. It is believed that the duration does not significantly change, once the flow pattern is established. In the test carried out for this research, the test area was relatively small and, hence, establishing the flownet did not need too much time.

In addition to the test pressure, the type of concrete also affects the duration of establishing a steady state of air flow. When the results in **Figure 7-a** and **7-b** are compared, the air flow for AC becomes stable within 10 minutes, whereas the air flow for MC needs around 20 minutes to achieve a similar stage. Various researchers [23, 27, 41] have shown that a more permeable concrete needs less time to establish a steady state of flow. The magnitude of the flow variations positively relates to the values of the corresponding flow rates, which agrees well with previous studies [4, 11, 42].

It may be noted that air can flow deeper under steady state test methods than that under non-steady state test methods. The investigation by Whiting and Cady [23] has shown that the air flow can be detected from 30 mm deep concrete, whereas research carried out by Schonlin and Hilsdorf [29], Torrent [9] and Basheer et al. [11] indicate that only the top layer (less than 20 mm) were examined by the non-steady state, falling head test methods. Therefore, another advantage of the steady state test is its ability to assess the overall quality of the near-surface concrete.

6.2 Relationship between steady-state flow rate and test pressure

Figure 8 shows the steady state flow rate against the test pressure. It can be seen that the steady-state flow rate strongly depends on the concrete curing regimes and this effect increases as the testing pressure is increased. As the pressure was increased from 0.5 bar to 2 bar, the flow rate increased from 0.42 to 14.12 µl/min for MC and from 0.47 µl/min to 31.50 µl/min for AC. Furthermore, the flow rates

of both concretes at 0.5 bar were extremely low, and it is not sufficient to distinguish the difference between the two concretes. This can be explained, because under the low test pressure air moves slowly, which performs more like a molecular diffusion dominated process instead of a pressure dominated process and using only Darcy's theory to evaluate the air transport coefficient might not be effective, especially for low pressure and low permeability [10, 22, 32, 43]. The difference in flow rates increases when the test pressure is above 1.2 bar.

The primary aim of this study was to determine the air permeability coefficient using the proposed approach. The formula (Eq 1) represents the relationship between air permeability coefficient and steady state air flow rate. To illustrate the procedure, an example of calculation is provided below:

- Environmental conditions in the laboratory: Temperature 21.5 ^{o}C; Relative humidity 62%.
- Curing regime: air cured (AC).
- Initial moisture condition: 40^{o}C dried for 28 days
- Age of concrete: 118 days [curing (90 days) + drying (28 days)]
- Test parameters:

  Radius of the test area: 0.025 m

  Calibration factor: $\frac{n_d}{n_f} \times \frac{l}{rb} = 0.051$ m^{-1} determined from the flow net

- Pressure applied: H=2 bar (20.4 m)
- Steady state flow rate:

  Q_{air}=66.95×10^{-9} m^3/min=1.116×10^{-9} m^3/s, as shown in **Table 3**.

- Calculation of the air permeability:

$$K_{air} = Q_{air} \times \frac{1}{2\pi h_t} \times \frac{n_d}{n_f} \times \frac{l}{rb} = \frac{1.116 \times 10^{-9}}{2 \times 3.14 \times 20.4} \times 0.051 = 4.443 \times 10^{-13} \text{ m/s}$$

The above procedure allows to examine the influence of test pressure on the estimated air permeability coefficient and the results are shown in **Figure 8-b**. As expected, the permeability coefficient estimated is a function of the test pressure. More importantly, the difference between MC and AC cannot be

clearly identified at the pressure of 0.5bar and a significant increase in the air permeability coefficient was obtained when pressure was raised above 1.2bar, beyond which the change is relatively non-significant, especially for the relatively high permeable concrete (AC). This suggests that the air permeability coefficient becomes independent on the test pressure applied. Combining with the requirements for site applications, the test pressure should be as low as possible in order to minimise the holding pressure needed to seal the test head on the surface and, hence, 2 bar is selected as the test pressure for the proposed test method.

6.3 Repeatability and capability of the new in situ steady state air permeability test

The error of the proposed steady state in situ air permeability test was assessed by repeating the air permeability measurements at the same location for 10 times [16, 24, 26]. After each measurement, the test set-up was disassembled and the measurement was repeated after 1 hour, allowing the pressure built up caused by the previous test to dissipate. To assess the distribution of the flow rate data, the Ryan-Joiner test was applied before carrying out further statistical analysis [25, 26], as shown in **Figure 9**. Obviously, the data points are close to the regression line and the p-value is higher than 0.1. This means that data are normally distributed and can be safely fed into the control charts without any transformation.

Figure 10 shows the control charts of the steady state air flow rates and its moving range (MR). As shown in the figure, all data points appear homoscedastic, staying within the upper and lower control limits. With respect to the moving range chart (**Figure 10-b**), the moving ranges are randomly distributed in the range from 0 to 1.38 µl/min within the control limits. It suggests that the conditions were under control in the process [16, 24, 26] and the average value of air flow rate can be considered as 22.06 µl/min, falling in the range of 20.94 µl/min (lower control limit) to 23.18 µl/min (upper control limit).

The next task was to justify whether the identified level of repeatability affects the conclusions derived from measurements. Two parameters, SNR and DR, were determined. The procedure to calculate these two indicators requires the ratio of concrete variability to total variability, as reported in our previous

study [15]. The total variability was evaluated by the average variance of ten replicates at different locations for AC and MC. After estimating the variability of measurements, the variability due to concrete can be determined through total variability (variability from measurement and concrete). **Figure 11** shows the test results of 10 different locations of AC and MC. In comparison to results in **Figure 10**, the variability of successive measurements at one position is much less than variability of measurements across the concrete slab, as the latter represents a combined influence from concrete and the test method. The SNR and DR are 14 and 193 respectively, which satisfy requirements of AIAG [25] and Montgomery [26]. As such, the repeatability of the proposed air permeability test method is acceptable to distinguish performance levels between the two different curing regimes.

The reliability of the proposed test method was examined by comparing the results obtained (steady state air flow rate) and water penetration depth obtained from the BE-EN water penetration test. No attempt is made to calculate the water permeability coefficient from the water penetration depth because an intrinsic property cannot be estimated from the measurements due to the influence of assessable porosity on calculated permeability coefficients. As shown in **Table 3**, the average air flow rates range from 0.42 µl/min to 66.95 µl/min, whilst the water penetration varied from 5.10 mm to 31.40 mm. That is, a similar conclusion can be obtained for both methods. This agreement was also reported by Whiting and Cady [23] and Bamforth [22] during their study on the relationship between air permeability and water permeability.

7. Conclusions

In this study, a steady-state field test was developed to assess the air permeability of the near-surface concrete. On the basis of numerical simulation and experimental results, the following conclusions have been drawn:

1) The influence of the key design parameters, such as depth of the specimen, testing area, seal size, on the calibration factor was assessed. The calibration factor is extremely sensitive to a change of the testing area which defines the overall flow area, whilst other factors, including the size of the

seal, the thickness of the specimen, and the width of the specimen, do not affect the calibration factor significantly.

2) The calibration factor increases as the thickness of the specimen increases and hence, correction to the calibration factor should be applied to assess the coefficient of air permeability. However, the value of calibration factor becomes constant (0.051 m^{-1}) if the depth of the specimen is greater than 50 mm. It is also noted that the distance to the outer side of the seal does not have a significant influence on the calibration factor.
3) Two stages of air flow can be identified from the experiments: (a) Non-steady state stage, marked by a significant fluctuation of flow rate; (b) Steady state stage, shown as a nearly constant flow rate. The duration to obtain a steady air flow rate depends on the pressure applied and the quality of the concrete investigated. In addition, flow rates stabilised around 15 minutes, suggesting that a site measurement can be completed within 20 minutes.
4) The steady air flow rate is nearly proportional to the test pressure if the pressure is above the threshold value of 0.5 bar and, more importantly, the difference in air flow rate at 0.5 bar is indistinguishable between the two concretes in this research. To enlarge the difference in flow rates between the two concretes, a test pressure of 2 bar is recommended for the steady state air permeability measurements.
5) The results of the repeatability experiment indicate that the variation of individual measurements is within 3 µl/min. As the SNR and DR of the method are 14 and 193 respectively, it can be concluded that the repeatability of the test does not significantly affect the conclusion.
6) By merely substituting the steady-state air flow rate into the proposed equation, one obtains the air permeability coefficient. As such, this technique provides a simple, but powerful tool to assess the possible durability of structural concrete.
7) It needs to be pointed out that this study mainly focuses on the development of a steady state air permeability test method and the specimens tested were preconditioned before measurements. As the moisture in concrete can significantly affect the air permeability test results and in order to obtain a reliable estimation of air permeability on site, the proposed test technique should be used along with relative humidity measurements. According to conclusions reported in previous

studies, the relative humidity within 20mm depth from the concrete surface should be lower than 75%.

Acknowledgement

The experiments described in this paper were carried out at the concrete laboratory of Chongqing University, which the authors gratefully acknowledge. The authors thank financial support provided by National Key R&D Program of China (No. 2017YFB0309900), National Natural Science Foundation of China (NO. 51878102 and 51520105012) and the Open Research Funds for the Shenzhen University, State Key Laboratory of High Performance Civil Engineering Materials and Chongqing Science Foundation Programme. The support from both the University of Leeds and Queen's University Belfast to complete this manuscript is highly appreciated.

Reference

[1] Vejmelková E, Koňáková D, Scheinherrová L, Doleželová M, Keppert M, Černý R. High temperature durability of fiber reinforced high alumina cement composites. Construction and Building Materials. 2018;162:881-91.
[2] Zhang Y, Zhang M, Ye G. Influence of moisture condition on chloride diffusion in partially saturated ordinary Portland cement mortar. Materials and Structures. 2018;51(2).
[3] Zhang P, Wittmann FH, Vogel M, Müller HS, Zhao T. Influence of freeze-thaw cycles on capillary absorption and chloride penetration into concrete. Cement and Concrete Research. 2017;100:60-7.
[4] Neves R, Branco F, Brito J. About the statistical interpretation of air permeability assessment results. Materials and Structures. 2011;45(4):529-39.
[5] Yang K, Basheer PAM, Bai Y, Magee BJ, Long AE. Development of a new in situ test method to measure the air permeability of high performance concretes. NDT & E International. 2014;64:30-40.
[6] Parrott LJ, Hong CZ. Some factors influecing air permeation measurements in cover conrete. Materials and Structures. 1991;24:403-8.
[7] Glanville, W.H., The permeability of portland cement concrete, Building Research Establishment, Technical paper, No. 3, 1931, 62 pp.
[8] Figg JW. Methods of measuring the air and water permeability of concrete. Magazine of Concrete Research. 1973;25:213-9.
[9] Torrent RT. A two-chamber vacuum cell for measuring the coefficient of permeability to air of the concrete cover on site. Materials and Structures. 1992;25:358-65.
[10] Dhir RK, Hewlett PC, Brars EA, Shaaban IG. A new technique for measuring the air permeability of near-surface concrete. Magazine of Concrete Research. 1995;47:167-76.
[11] Basheer PAM, Montgomery DC, Long A. 'CLAM' tests for measuring in-situ permeation properties of concrete. NDT & E International. 1995;12:53-73.
[12] Torrent RT, Alexander MG, Kropp J. Introduction and problem statement. Non-Destructive Evaluation of the Penetrability and Thickness of the Concrete Cover RILEM TC 189-NEC: State-of-the-Art Report: RILEM; 2007.
[13] Yang Z, Fischer H, Polder R. Synthesis and characterization of modified hydrotalcites and their ion exchange characteristics in chloride-rich simulated concrete pore solution. Cement and Concrete Composites. 2014;47:87-93.
[14] Liu J, Agostini F, Skoczylas F. From relative gas permeability to in situ saturation measurements. Construction and Building Materials. 2013;40:882-90.

[15] Imamoto K, Shimozawa K, Nagayama M, Yamasaki J, Nimura S. Threshold values of air permeability of concrete cover - A case study in Japan. On site assessment of concrete, masonry and timber structures. Varenna Como Lake, Italy2008. p. 169-77.
[16] Yang K, Basheer PAM, Magee B, Bai Y, Long AE. Repeatability and Reliability of New Air and Water Permeability Tests for Assessing the Durability of High-Performance Concretes. Journal of Materials in Civil Engineering. 2015;27(12).
[17] Hall C. Water sorptivity of mortars and concretes a review. Magazine of Concrete Research. 1989;41:51-61.
[18] Claisse P, Elsayad HI, Shaaban IG. Test Methods for Measuring Fluid Transport in Cover Concrete. Journal of Materials in Civil Engineering. 1999;11(2):138-43.
[19] Yang K, Basheer PAM, Bai Y, Magee BJ, Long AE. Assessment of the effectiveness of the guard ring in obtaining a uni-directional flow in an in situ water permeability test. Materials and Structures. 2015;48(1):167-83.
[20] Basheer PAM. Permeation analysis. In: V.S. R, Beaudoin JJ, editors. Handbook of Analytical Techniques in Concrete Science and Technology: Principles, Techniques and Applications: Noyes Publications; 2001. p. 658-727.
[21] Adams AE. Development and application of the CLAM for measureing concrete permeability. Belfast: Queen's University Belfast; 1986.
[22] Bamforth PB. The relationship between permeability coefficients for concrete obtained using liquid and gas. Magazine of concrete research. 1987;39(138):3 –11.
[23] Whiting D, Cady PD. Condition Evaluation of Concrete Bridges Relative to Reinforcement Corrosion. Washington, D.C.: Strategic Highway Research Program; 1992. p. 93.
[24] ISO-5725. Accuracy (trueness and precision) of measurement methods and results. Part-2: Basic methods for the determination of repeatability and reproducibility of a standard measurement method. ISO; 1994. p. 62.
[25] AIAG. Measurement system analysis: Reference manual. MI2002.
[26] Montgomery DC. Statistical quality control: A modern introduction. 6th ed. Oxford, England: Wiley; 2009.
[27] Arbaoui T. Finite element calibration of the CLAM: Queen's University Belfast; 1988.
[28] Rawlings JO, Pantula SG, Dickey DA. Applied regression analysis: A research tool. 2nd ed: Springer; 1998.
[29] Schonlin K, Hilsdorf HK. Evaluation of the effectiveness of curing of concrete structures. In: Scanlon JM, editor. Concrete Durability: Katharine and Bryant Mather International Conference: ACI; 1987. p. 207-26.
[30] Yang K, Yang CH, Long A, Basheer PAM. Use of two-pressure-head method to assess water permeability of structural concrete. ACI Materials Journal. 2018;115(1):65-75.
[31] Basheer L, Kropp J, Cleland DC. Assessment of the durability of concrete from its permeation properties: a review. Construction and Building Materials. 2001;15:93-103.
[32] Harris AW, Atkinson A, Claisse PA. Transport of gases in concrete barriers. Waste Management 1992;12:155-7.
[33] Ballim Y. Curing and the durability of OPC, fly ash and blast-furnace slag concretes. Materials and Structures. 1993;26:238-44.
[34] Yang K. Development of a new field permeability test method to assess the durability of low permeable concrete: Queen's University Belfast; 2012.
[35] BS:1881-125. Methods for mixing and sampling fresh concrete in the laboratory. London: BSI; 1986. p. 1-10.
[36] GB/T-50082. Standard for test methods of long-term performance and durability of ordinary concrete. MOHURD; 2009. p. 51.
[37] Yang K, Basheer PAM, Magee BJ, Bai Y. Investigation of moisture condition and Autoclam sensitivity on air permeability measurements for both normal concrete and high performance concrete. Construction and Building Materials. 2013;48:306-14.
[38] Parrott LJ. Moisture conditioning and transport properties of concrete test specimens. Materials and Structures. 1994;27:460-8.
[39] BS EN: 12390-8. Testing hardened concrete. Depth of penetration of water under pressure. London: BSI; 2009. P. 1-210.
[40] El-Dieb AE, Hooton RD. water permeability measurement of high performance concrete using a high pressure triaxial cell. Cement and Concrete Research. 1995;25:1199-208.
[41] Dhir RK, Hewlett PC, Chan YN. Near-surface characteristics of concrete assessment and development of in situ test methods. Magazine of Concrete Research. 1987;39:183-94.
[42] Denarie E, Jacobs F, Leemann A, Teruzzi T, Torrent RT. Specification and site control of the permeability of the cover concrete: the Swiss approach. In: Leung C, Wan KT, editors. International RILEM Conference on Advances in Construction Materials Through Science and Engineering: RILEM Publications SARL; 2011. p. 478 - 85.

[43] Bear J. Dynamics of fluid in porous media. New York: American Elsevier; 1972.

Table and Figure

Table 1 Design of factorial experiment to assess the influence of different factors on calibration factor
Table 2 Estimated effects and coefficients for calibration factor
Table 3 Results of steady state air permeability test and water penetration test

Figure 1 Illustration of determining the calibration factor through the flow patterns
Figure 2 Geometry considered for air flow models to study influence of test arrangements on calibration factor
Figure 3 Main effects plots of the factors for l/rb
Figure 4 Air flow simulation of different specimen configurations
Figure 5 Calibration factor under different specimen depths and distances to outer ring
Figure 6 Test set up of the new air permeability test device
Figure 7 Air flow rates under different testing pressure
Figure 8 Influence of test pressure on steady state air flow rate and air permeability coefficient (K_{air})
Figure 9 Probability plot for bias and Ryan-Joiner test for normal distribution
Figure 10 Control charts for bias and moving range (MR) of the new air permeability test
Figure 11 As received test results from the field air permeability test

Table 1 Design of factorial experiment to assess the influence of different factors on the calibration factor

Factor / level	d_{sp} (mm)	w_{sp} (mm)	r_{ta} (mm)	s_w (mm)
"+"	100	150	25	10
"-"	50	100	50	30

Note: 1) d_{sp} = specimen depth; lower level of 50mm based on flownet simulation by Arbaoui [27] to prevent the influence of thickness on rate of air flow, upper level of 100mm based on the largest thickness influencing the flownet.
2) w_{sp} = distance to the edge of the specimen from the centre of the test area; the lower and upper levels selected considering the possible arrangement of test locations and additional area for expansion bolts to hold the test head on the concrete surface.
3) r_{ta} = radius of the test area; lower level of 25 mm (giving a diameter of 50mm) to eliminate the influence of size of coarse aggregate (assuming this to be 20mm for most concretes) on flow rates, upper level was kept at 50mm (giving a diameter of 100mm) to ensure that the force required to seal the test head is practically manageable on site.
4) S_w = size of seal; lower level of 10mm selected such that this is the lowest width of the seal to ensure the air flow to be perpendicular to the test surface, the upper level of 30mm was chosen to ensure that most of the air flow is perpendicular to the test surface.

Table 2 Estimated effects and coefficients for calibration factor

Term	Effect	Coef	Standard error Coef	t-test Value	P-Value
Constant		0.0325	0.0008	40.56	0.016*
r_{ta}	-0.0266	-0.0133	0.0008	-16.64	0.038*
s_w	0.0038	0.0019	0.0008	2.37	0.254
d_{sp}	0.0033	0.0017	0.0008	2.07	0.287
w_{sp}	-0.0015	-0.0007	0.0008	-0.92	0.525
$r_{ta}\times s_w$	-0.0020	-0.0010	0.0008	-1.25	0.429
$r_{ta}\times d_{sp}$	0.0008	0.0004	0.0008	0.51	0.698
$r_{ta}\times w_{sp}$	0.0001	0.0001	0.0008	0.07	0.952
$s_w\times d_{sp}$	-0.0002	-0.0001	0.0008	-0.11	0.929
$s_w\times w_{sp}$	0.0028	0.0014	0.0008	1.77	0.327
$d_{sp}\times w_{sp}$	0.0014	0.0007	0.0008	0.85	0.553
$r_{ta}\times s_w\times d_{sp}$	0.0002	0.0001	0.0008	0.12	0.926
$r_{ta}\times s_w\times w_{sp}$	0.0007	0.0004	0.0008	0.44	0.737
$r_{ta}\times d_{sp}\times w_{sp}$	-0.0012	-0.0006	0.0008	-0.73	0.600
$r_{ta}\times s_w\times d_{sp}\times w_{sp}$	0.0007	0.0003	0.0008	0.43	0.743

Note: * Effect significant, P-value 1-5%.

Table 3 Results of steady state air permeability test and water penetration test

Test method	Pressure applied (bar)	Permeability test	
		MC	AC
Field steady state air permeability test	0.5	0.42 µl/min	0.47 µl/min
	1.2	14.12 µl/min	31.50 µl/min
	2.0	41.98 µl/min	66.95 µl/min
BS-EN water penetration test	7.0	5.10 mm	31.40 mm

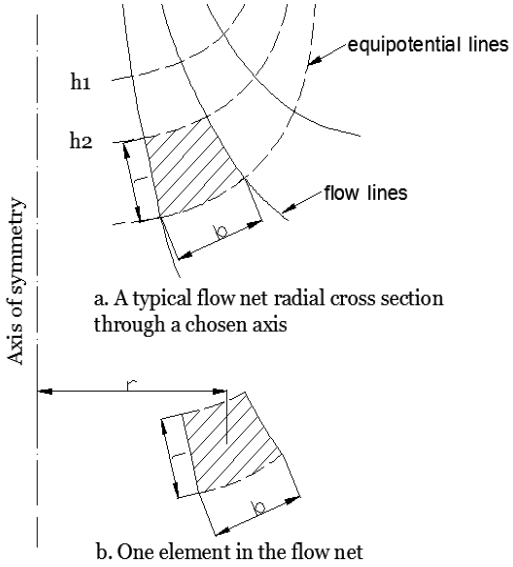

Figure 1 Illustration of determining the calibration factor through the flow patterns

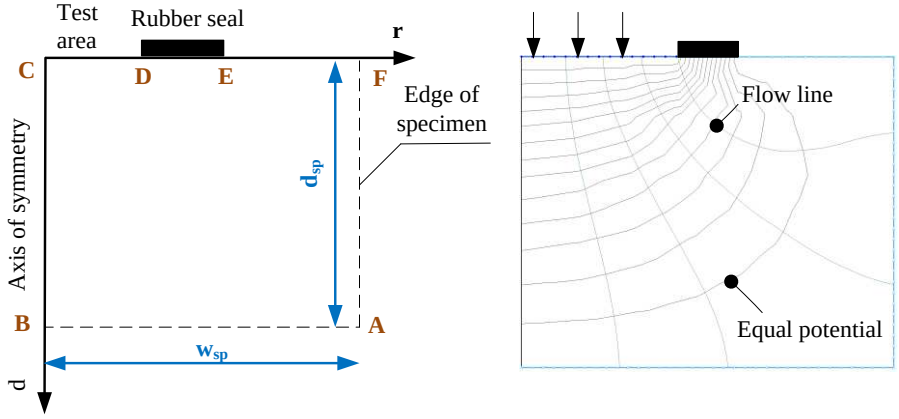

(a) Geometry considered for air flow models

(b) Output of air simulation model

Figure 2 Geometry considered for air flow models to study influence of test arrangements on calibration factor (Initial and boundary condition: 1. BA, AF, FE-zero potential; ED, CB-now flow, DC-constant head head)

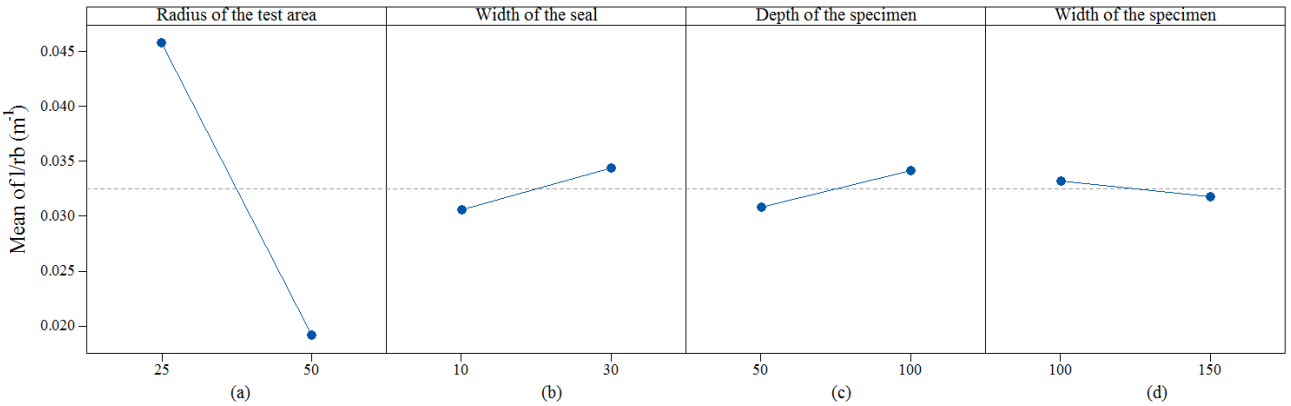

Figure 3 Main effects plots of the factors for l/rb

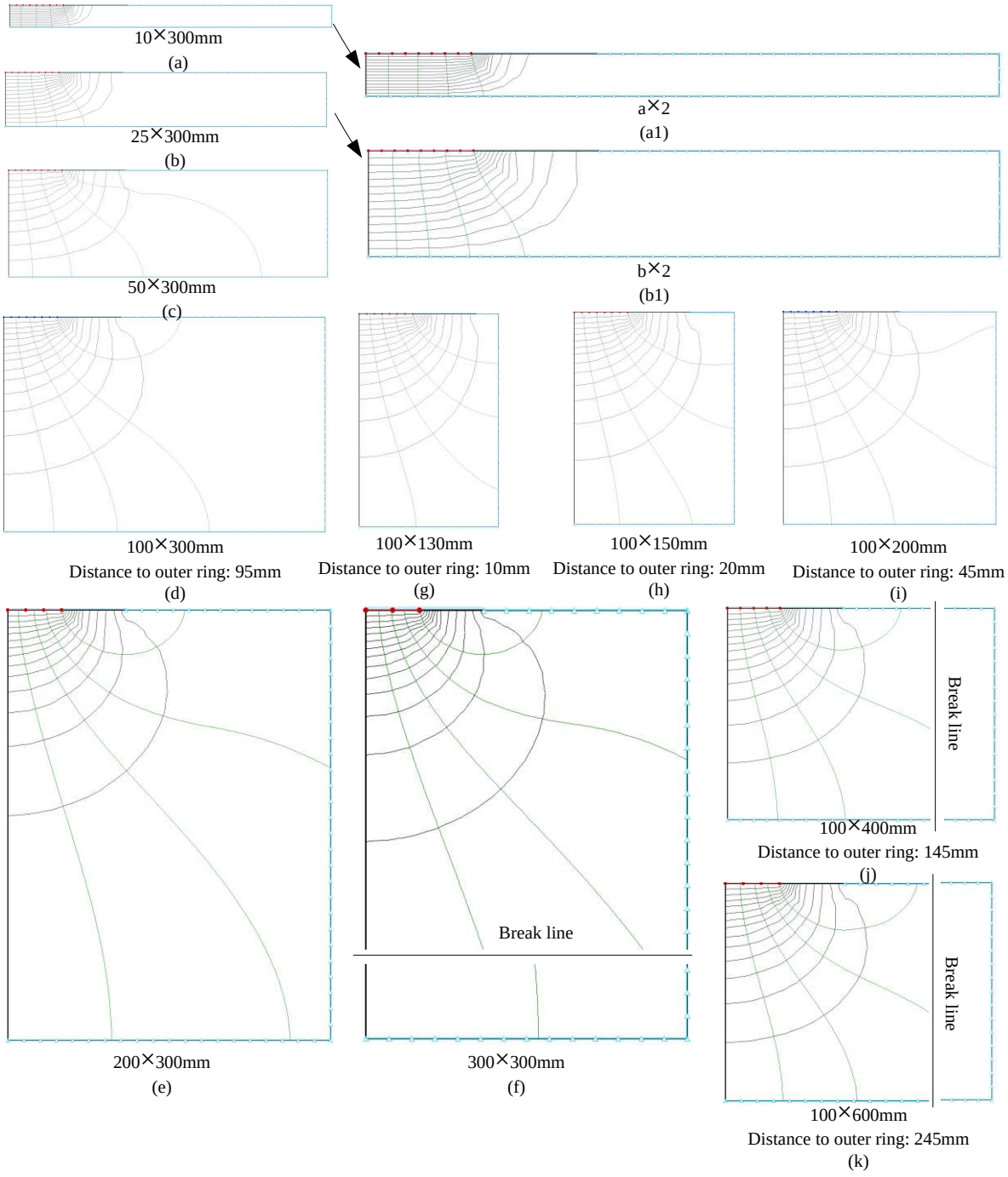

Figure 4 Air flow simulation of different specimen configurations

Note: 1) The width was kept constant at 300mm when the influence of the depth on calibration factor was assessed; 2) The depth was kept at 100mm when the influence of the distance to the outer ring was assessed.

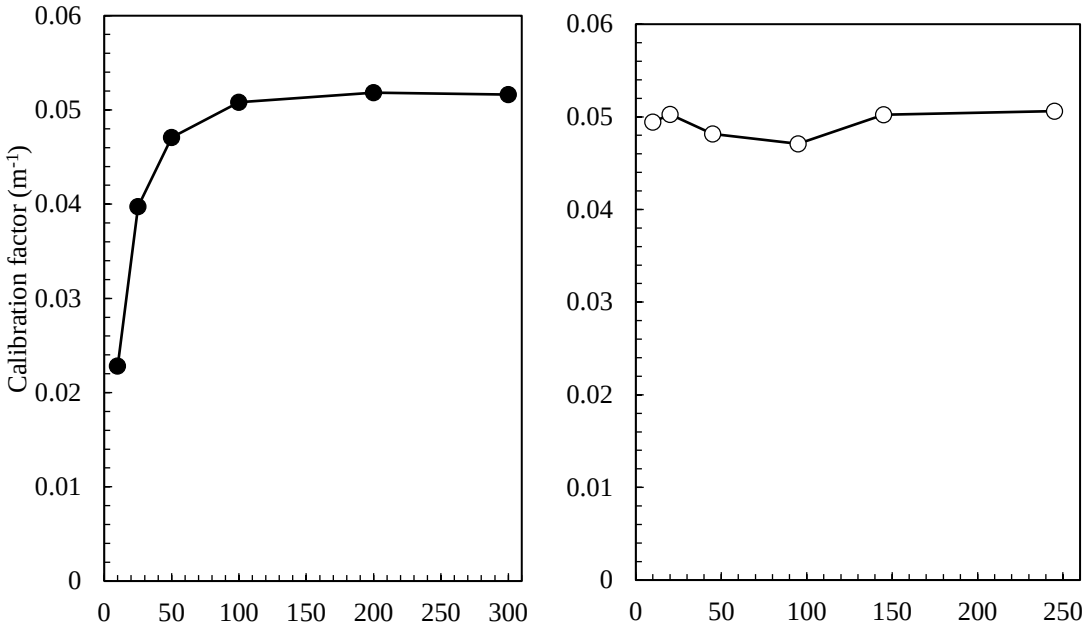

(a) Depth of specimen (mm) (b) Outer edge of the specimen (mm)

Figure 5 Calibration factor under different specimen depths and distances to outer edge of the specimen

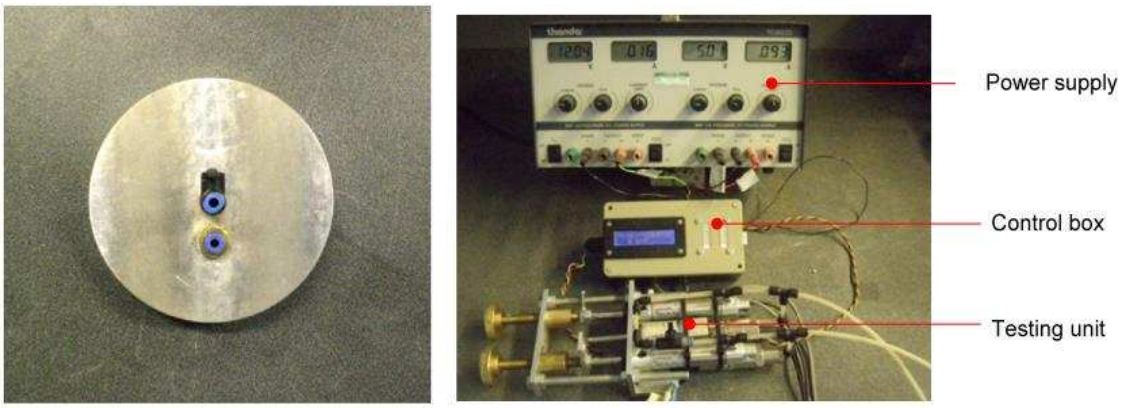

(a) top view of test head (b) Main body of permeability test

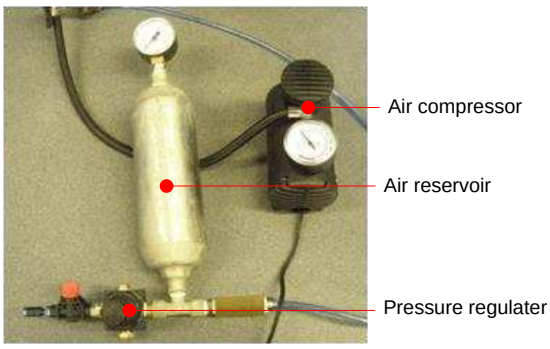

(c) The priming system

Figure 6 Test set up of the new air permeability test device

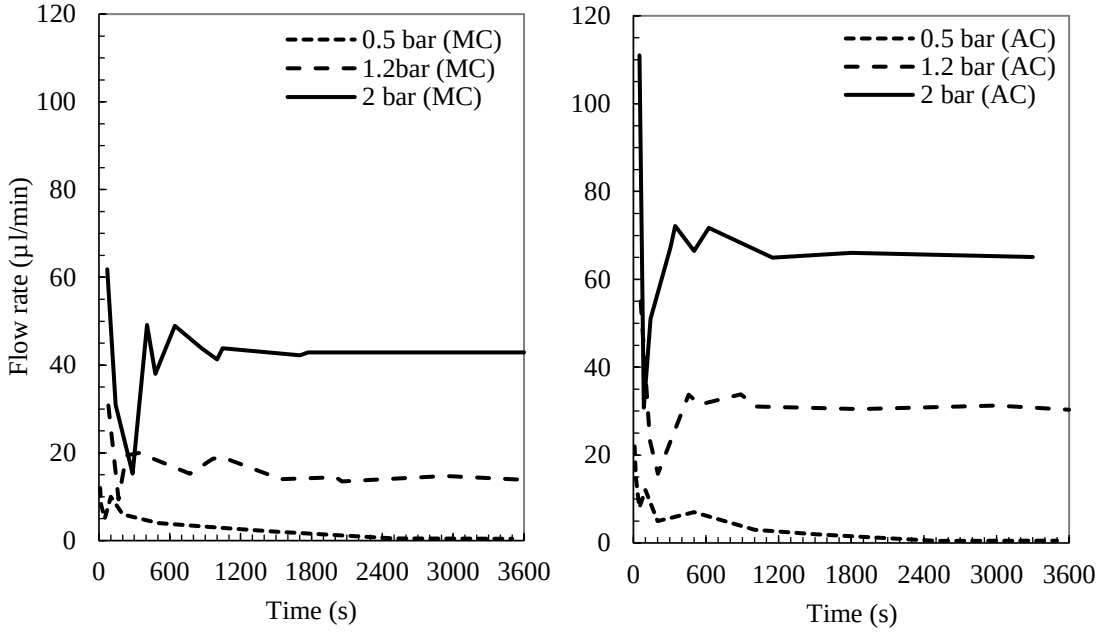

(a) Flow rate Vs time: MC (b) Flow rate Vs time: AC

Figure 7 Air flow rates under different testing pressure

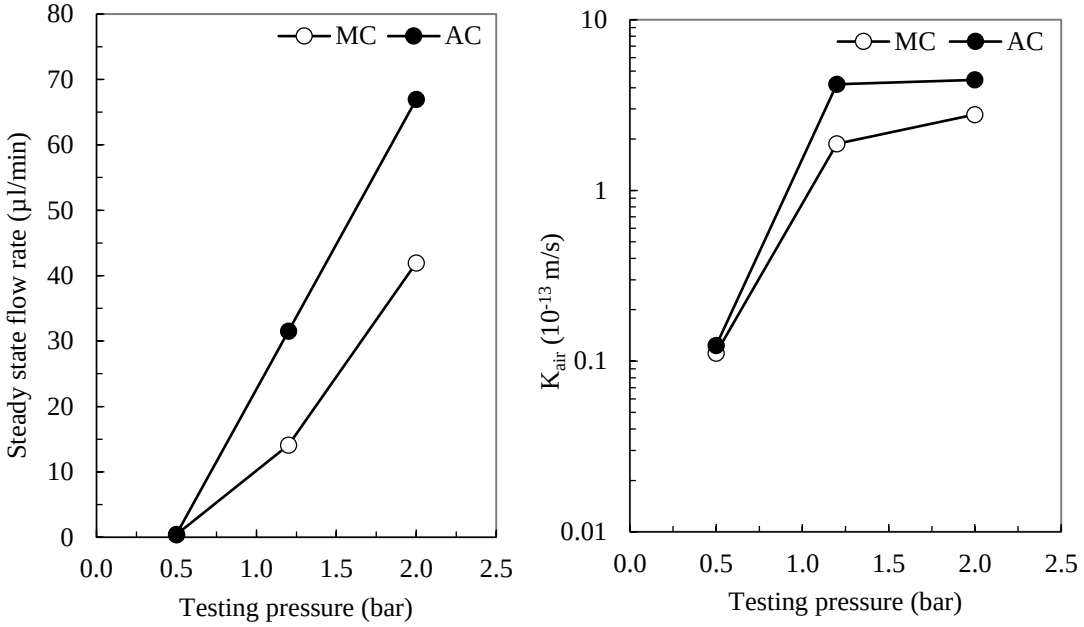

(a) Flow rate Vs test pressure (b) K_{air} Vs test pressure

Figure 8 Influence of test pressure on steady state air flow rate and air permeability coefficient (K_{air}) (The air flow rates at different pressure was converted to the flow rates at 1 atm)

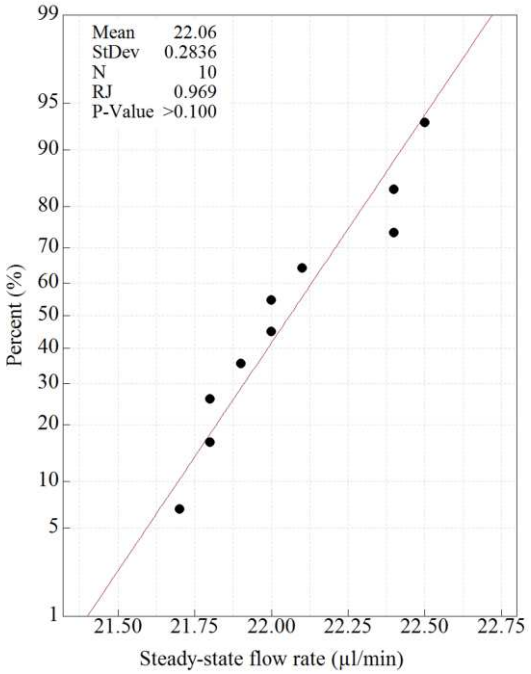

Figure 9 Probability plot for bias and Ryan-Joiner test for normal distribution

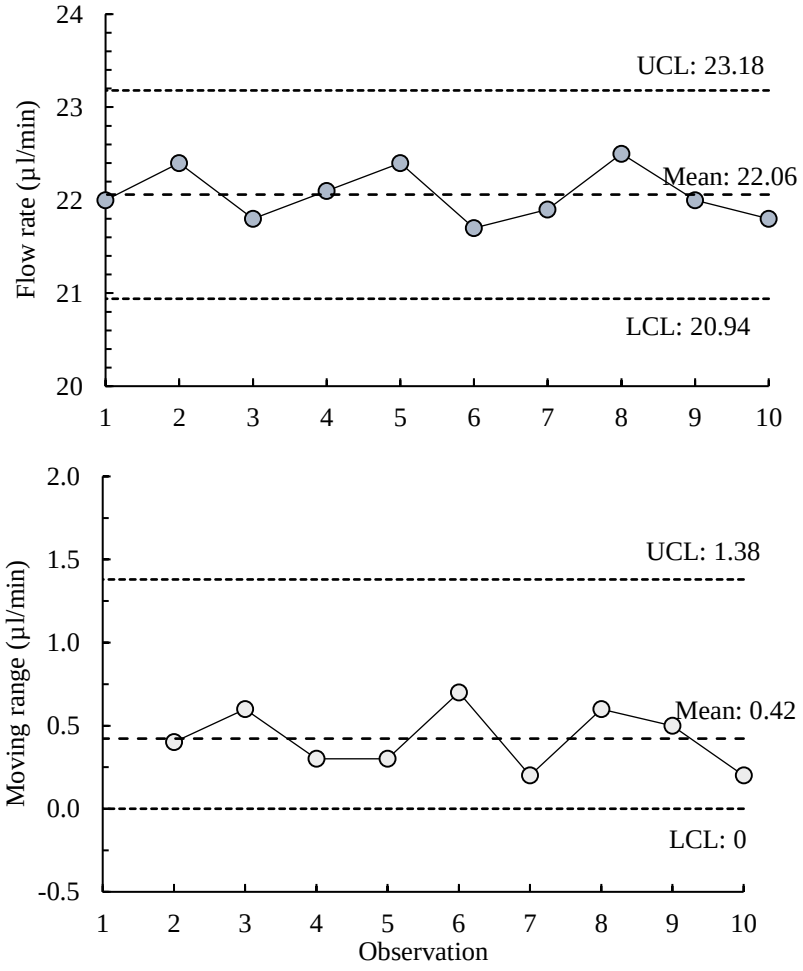

Figure 10 Control charts for bias and moving range (MR) of the new air permeability test (measurements taken on the same location)

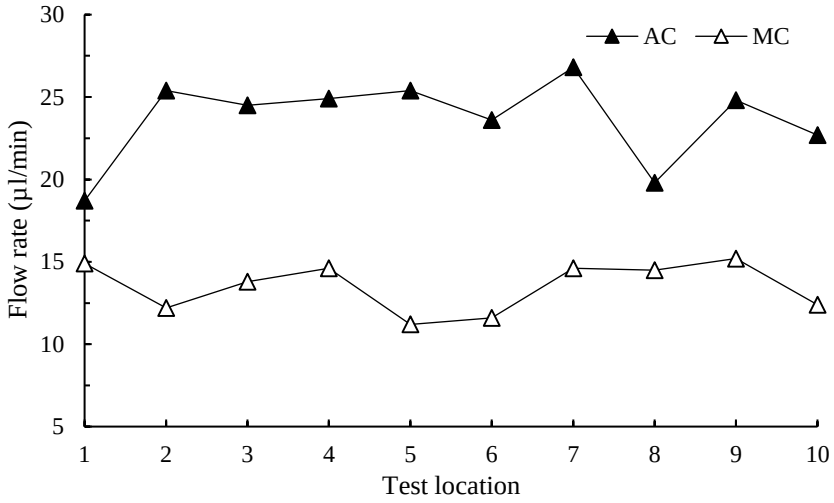

Figure 11 As received test results from the field air permeability test